Chemical Papers (2022) 76:1875–1884
https://doi.org/10.1007/s11696-021-01982-4

ORIGINAL PAPER

Preparation of graphitic carbon nitride g-C_3N_4-HMCM-22 composite catalysts and enhanced para-selectivity in m-xylene isomerization

Zonghui Liu[1] · Zhongze Zhang[1] · Dehua Xie[1] · Xiaotian Guan[1] · Fei Wang[1] · Bing Xue[1]

Received: 31 May 2021 / Accepted: 11 November 2021 / Published online: 28 January 2022

Abstract

A series of novel graphitic carbon nitride g-C_3N_4-HMCM-22 composite catalysts were successfully prepared. Their structure and acid properties were well characterized by thermogravimetric analysis (TGA), X-ray diffraction (XRD), N_2 adsorption–desorption, Fourier transform infrared spectroscopy (TFIR), X-ray photoelectron spectroscopy (XPS), Scanning Electron Microscopy (SEM), and Py-FTIR. The prepared g-C_3N_4-HMCM-22 composite catalysts were then used for m-xylene (MX) isomerization. The effect of introduction of g-C_3N_4 on catalytic performance was studied. Compared with parent HMCM-22 catalyst, g-C_3N_4-HMCM-22 composite catalysts exhibited an improved p-xylene (PX) selectivity in MX isomerization. Moreover, G1H1 composite catalyst showed the highest PX selectivity than other as-prepared composite samples. Correlating the catalyst performance with its physical and chemical properties uncovers that increasing amounts of Lewis acid sites and effectively inhibiting the external Brönsted acid sites of HMCM-22 would be the key to improving the selectivity of PX.

Keywords m-xylene · p-xylene · Isomerization · g-C_3N_4-HMCM-22 catalyst

Introduction

Para-xylene (*p*-xylene, PX) was one of the three isomers of xylene, which is often used as industrial solvents or intermediates for many derivatives, such as terephthalate and polyester (Tsai et al. 2007; Shi et al. 2018). Nevertheless, conventional synthetic methods of PX had been much limited due to high-cost and harsh reaction conditions required (Araujo et al. 2001). Therefore, many continuous efforts had been made to reduce the production cost of PX and improve PX yield and selectivity (Wu et al. 2016). The selective synthesize of PX by *m*-xylene (MX) isomerization was proved to be an effective method to increase the production to meet the increasing industrial demand (Zhou et al. 2013; Min et al. 2012).

MX isomerization was a commendable reaction of acid catalysis that was generally used as a model reaction for acidity adjustment (Jeong et al. 2009; Yeong et al. 2010). Zeolites, a class of microporous crystalline materials with highly defined porous structures due to their unique framework structures (Dusselier et al. 2018), high cation-exchange capacities (Shamzhy et al. 2019), good adsorptivities (Li et al. 2014), and moderate acidities (Bailleul et al. 2019), as the most important solid catalysts, had attracted a substantial interest in the chemical industry (Weston at al. 2019). So far, many kinds of zeolites, such as mordenite (He et al. 2020) and Y (Miao et al. 2020), clinoptilolite (Ghasemian et al. 2014), and beta (Qi et al. 2020) had been applied in many petrochemical reactions. Among them, MCM-22 had the particularity to contain two independent noninterconnected pore systems, each accessible through 10-membering (MR) apertures and 12-MR pockets on the external surface (Amin et al. 2017). Many reactions were investigated over protonated samples (HMCM-22) showing that the behavior of this zeolite was intermediate between those of 12-MR (large pore) and 10-MR (average pore) zeolites (Ayrault et al. 2004; Wang et al. 2015a, b). The coexisting pore systems of HMCM-22 provided high thermal stability, high acid-catalyzed activity and shape selectivity for excellent catalytic performance in alkylation (Wang et al.

✉ Zonghui Liu
liuzh@cczu.edu.cn

✉ Bing Xue
xuebing@cczu.edu.cn

[1] Jiangsu Key Laboratory of Advanced Catalytic Materials and Technology, School of Petrochemical Engineering, Changzhou University, Gehu Middle Road 21, Changzhou 213164, Jiangsu, People's Republic of China

2018), catalytic cracking (Wang et al. 2015a, b), isomerization (Shang et al. 2008), disproportionation (Wu et al. 1998), and so on. Ma et al. reported that a hierarchical MCM-22 material with microporous–mesoporous structure was found to be a highly efficient solid acid catalyst for the liquid phase isomerization of β-pinene, which can achieve 100% conversion of β-pinene and 93.7% yield for main products under mild reaction conditions (Ma et al. 2017).

Modification was a highly efficient method for improving the para-selectivity by reducing the external acid sites and adjusting the pore entrance (Wang et al. 2012; Zhang et al. 2013). Xue et al. reported a MgO-modified MCM-22 catalyst, which was ascribed to suppression of xylene isomerization by reduction in the external surface Brönsted acid sites (Xue et al. 2009). Here, we also reported a series of novel graphitic carbon nitride composite catalysts (g-C_3N_4-HMCM-22), which were successfully prepared using dicyanamide (DCDA) as precursor and anhydrous ethanol as solvent and were characterized by X-ray diffraction (XRD), N_2 adsorption, Fourier transform infrared spectroscopy (FTIR), and X-ray photoelectron spectroscopy (XPS). Their catalytic performance for isomerization of MX, an important industrial reaction to produce PX, was investigated. For comparison, parent g-C_3N_4 and HMCM-22 as catalysts were also prepared for MX isomerization. The 50%g-C_3N_4-HMCM-22 catalyst was the most efficient catalyst and offered the PX selectivity as high as 77%. Based on physical and chemical properties analysis, increased amounts of Lewis acid sites and effective suppression of external Brönsted acid sites of G1H1 resulted in improved PX selectivity.

Experimental

Catalyst preparation

Synthesis of HMCM-22 zeolite: MCM-22 zeolites with Si/Al=50 were prepared by hydrothermal crystallization according to the reported procedure (Wu et Al. 2008). Then, MCM-22 zeolites were converted into HMCM-22 by ion-exchange with aqueous NH_4NO_3 solution. It was exchanged twice with a 2 M NH_4NO_3 solution, under stirring at 353 K for 1 h and calcined at 823 K for 4 h under airflow.

Synthesis of g-C_3N_4-HMCM-22 composite catalysts: the g-C_3N_4-HMCM-22 composite catalysts were prepared by an in situ method. In a typical process, a certain amount of dicyandiamide powder and anhydrous ethanol were mixed and stirred for 15 min. And the as-prepared molecular sieve (HMCM-22) was then immersed with above dicyandiamide solution and stirred under 363 K. Until all the alcohol evaporated and dried, the above mixture was put into a muffle furnace and then calcined for 2 h at 823 K with a heating rate of 15 K/min in static air. Finally, g-C_3N_4-HMCM-22 composite catalysts were prepared. The actual mass ratio of g-C_3N_4 to HMCM-22 was measured by TG analysis.

Characterization

Thermogravimetric analysis (TGA) was performed using a 209 F3 instrument, and 5–10 mg of the sample was employed for the measurement at temperatures from 50 to 800 °C, with a heating rate of 10 °C min^{-1} in air.

X-ray diffraction (XRD) measurements were conducted using a Rigaku D/max2500PC diffractometer with Cu Kα ($\lambda = 1.54$ Å) radiation. The diffractograms were recorded in 2θ range 5°–50° in steps of 0.02° with a count time of 15 s.

Nitrogen adsorption isotherms were measured at -196 °C using a Micromeritics ASAP 2020 analyzer. Before the analysis, the samples were degassed (1.33×10^{-2} Pa) at 423 K for at least 4 h. The specific surface area was calculated according to the Brunauer–Emmett–Teller (BET) isothermal equation. The pore diameter and pore size distribution were determined from the Horvath–Kawazoe (H–K) method.

Fourier transform infrared (FTIR) spectra of the samples were collected in transmission mode from KBr pellets at room temperature on a Bruker Tensor 27 spectrometer with a resolution of 4 cm^{-1}, using 32 scans per spectrum in the region of 400–4000 cm^{-1}. The Brönsted and Lewis acid sites were discriminated by FTIR spectra of pyridine adsorption (Py-FTIR). About 15 mg samples were pressed into self-supporting wafers, pretreated at 623 K under evacuation, and then absorbed pyridine at room temperature. After equilibration, the samples were evacuated at 473 K to remove the excess probe molecules. The quantities of Brönsted and Lewis acid sites were estimated in the range of 1400–1600 cm^{-1} for Py-FTIR.

X-ray photoelectron spectroscopy (XPS) measurements were performed using a Perkin-Elmer PHI 5000C spectrometer working in the constant analyzer energy mode with Mg Kα radiation as the excitation source.

Scanning electron microscopy (SEM) images were performed on a SUPRA55 instrument scanning electron microscope operated at 15 kV.

Catalytic test

Vapor phase isomerization of m-xylene (MX) reaction was performed in a plug flow reactor. For each experiment, about 1 g of the prepared catalyst in 20–60 mesh was packed in a fixed bed stainless steel reactor with an inner diameter of 1 cm. The feed gas components were controlled by mass flow controller. MX mixture was injected to the reactor at the top of the reactor by means of an infusion pump. Reaction products were sampled and analyzed online on gas chromatography (GC-6890A) fitted with an FFAP capillary column and a

flame ionization detector. The experiments were conducted at temperature in the range 623–723 K.

Results and discussion

Characterization of catalysts

According to the previous work reported by Groenewolt et al, g-C_3N_4 materials can be prepared from cyanamide (Groenewolt et al. 2005). The DSC thermogram was performed to study the process of g-C_3N_4 synthesis from cyanamide. First, the endothermic melting of cyanamide occurred at 45 °C, then converted to dicyandiamide at 150 °C via exothermic dimerization. The dicyandiamide melted (endothermic reaction) at 200 °C and converted to melamine at 240 °C by an exothermic reaction, followed by the endothermic reaction to melem at 390 °C, Finally, the melem converted to g-C_3N_4 at around 520 °C.

In order to verify the actual mass composition of g-C_3N_4-HMCM-22 composite catalysts, TG analysis of fresh composite catalysts, HMCM-22 and g-C_3N_4 was performed and the results are shown in Figure 1. The TG curves presented a significant weight loss when samples were heated from room temperature to 800 °C in air. In fact, the initial marginal weight loss (3–5 wt%) after heating to 150 °C was due to physisorbed water. For g-C_3N_4, a 96.4% weight loss was obtained over the temperature range of 400–700 °C, which is attributed to the combustion of g-C_3N_4. It is also indicated that the g-C_3N_4 could be completely burned up in air at 700 °C. The results agree well with the literature (Groenewolt et al. 2005). And obviously, there was no mass loss of HMCM-22 when the temperature increased from 200 to 800 °C (Fig. 1). This means that the mass loss of g-C_3N_4-HMCM-22 catalyst was all corresponding to the combustion of g-C_3N_4. Hence, we can calculate the composition of g-C_3N_4-HMCM-22 composite catalysts according to the mass loss of samples. The actual mass ratio of g-C_3N_4 to HMCM-22 was 1:9, 1:1 and 3:1. Therefore, the samples with these different mass ratios are denoted here as G1H9, G1H1, and G3H1, respectively.

Figure 2 shows XRD patterns of g-C_3N_4, HMCM-22 and as-prepared composite samples. The pure g-C_3N_4 showed two pronounced peaks at 27.4 ° and 13.2 ° which correspond to interlayer stacking of aromatic segments and tri-s-triazine units of g-C_3N_4 phase assigned to (100) and (002) planes, respectively (Xu et al. 2015). Typical diffraction lines of obtained HMCM-22 samples corresponding to the MWW structure agree well with the literature (Leonowicz et al. 1994), which were observed indicating that the HMCM-22 samples with pure phase and high crystallinity were obtained. After introduction of g-C_3N_4, the peak positions of MCM-22 were not changed and the new characteristic peaks of other crystalline phases or amorphous phases were also not observed. In addition, we found that the peaks corresponding to g-C_3N_4 were also absent with increasing g-C_3N_4 content of the composite samples. This may be because the HMCM-22 zeolite was perfectly incorporated into the g-C_3N_4 matrix.

The surface area and pore size analysis of parent HMCM-22 and as-prepared composite samples were studied by N_2 adsorption isotherm, as shown in Fig. 3. The HMCM-22 sample presented type I isothermal curves, indicating the existence of microporous structure in HMCM-22 zeolite, which also agrees well with the literature (Xue et al.

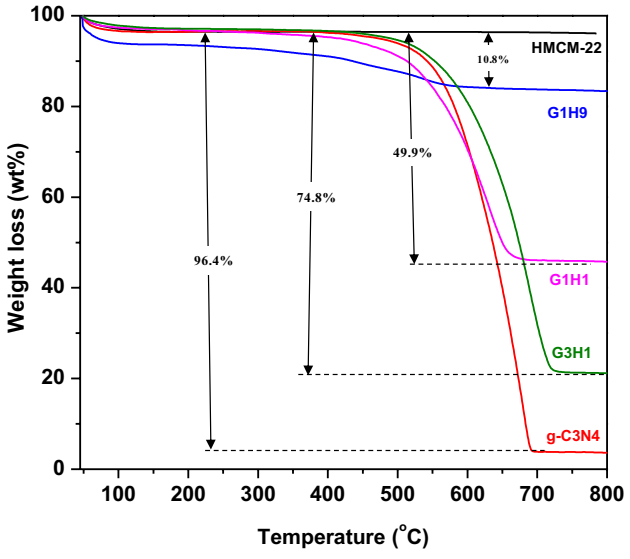

Fig. 1 TG curves of parent g-C_3N_4 and as-prepared composite samples

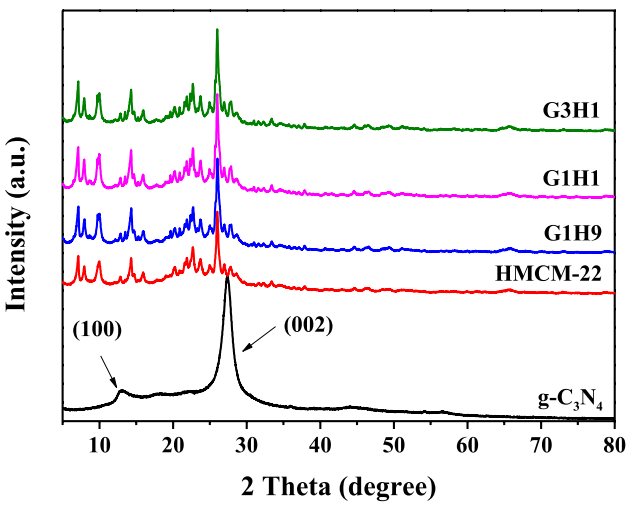

Fig. 2 XRD patterns of parent g-C_3N_4, HMCM-22 and as-prepared composite samples

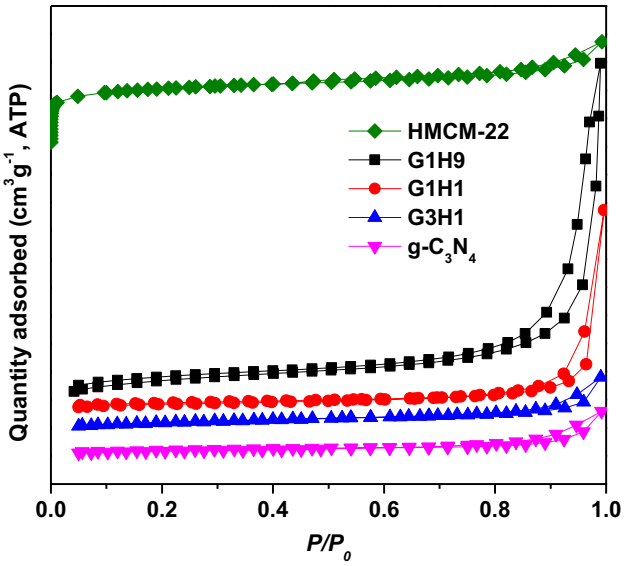

Fig. 3 N_2 adsorption–desorption isotherms of parent HMCM-22 and as-prepared composite samples

2014). The rest of the samples include g-C_3N_4 and g-C_3N_4-HMCM-22 showed the type IV isotherms with H1-shaped hysteresis loops in the relative pressure (p/p_0) ranging from 0.85 to 0.99, which were the characteristics of mesoporous structure (Chu et al. 2010). Furthermore, the detailed textural properties of parent HMCM-22 and as-prepared composite samples are summarized in Table 1. Parent HMCM-22 catalyst had the largest BET surface area of 292 $m^2\ g^{-1}$, as well as a highest total volume (0.25 $cm^3\ g^{-1}$) than other as-prepared composite samples. After introduction of small amount of g-C_3N_4 to HMCM-22, the BET surface area and pore volume of the G1H9 catalyst decreased to 186 $m^2\ g^{-1}$ and 0.19 $cm^3\ g^{-1}$, respectively. Further increase in g-C_3N_4 content of the composite samples, the BET surface area and pore volume of the G3H1 catalyst continued to decrease to 28 $m^2\ g^{-1}$and 0.07 $cm^3\ g^{-1}$. The g-C_3N_4 had the lowest

Table 1 Textural parameters of parent HMCM-22 and as-prepared composite samples

Catalysts	S_{BET}/$m^2\ g^{-1}$[a]	S_{mic}/$m^2\ g^{-1}$[b]	V_t/$cm^3\ g^{-1}$[c]	V_{mic}/$cm^3\ g^{-1}$[d]
HMCM-22	292	219	0.25	0.12
G1H9	186	95	0.19	0.05
G1H1	85	47	0.13	0.04
G3H1	28	11	0.07	0.01
g-C_3N_4	17	6	0.06	0.01

[a]S_{BET}: BET surface area

[b]S_{mic}: Micro-pore area

[c]V_t: Total pore volume

[d]V_{mic}: Micro-pore volume.

BET surface (17 $m^2\ g^{-1}$) and total volume (0.06 $cm^3\ g^{-1}$). In addition, it shows that similar trends were observed for micropore area and the micropore volume follows the trend of HMCM-22 > G1H9 > G1H1 > G3H1 > g-C_3N_4, which might be due to partial blockage on pore mouth and external surface of the pore system of MCM-22 for modification of g-C_3N_4. These results indicated that modification of g-C_3N_4 would perhaps lead to a better para-selectivity.

Figure 4 shows the FTIR spectra of g-C_3N_4, HMCM-22 and as-prepared composite samples. Adsorption bands at 1090 cm^{-1} and 1240 cm^{-1} were observed, which typically correspond to asymmetric stretching vibration of the T-O-T tetrahedron on HMCM-22, respectively. After introduction of g-C_3N_4, new peaks were found at 3156-3078 cm^{-1}, originating from the stretching mode of primary and secondary amine groups (Talapaneni et al. 2012) and the stretching and deformation vibration of the heterocyclic compound aromatic amines C–N and C=N of the multiple bands were formed in the range of 1600 cm^{-1} to 1200 cm^{-1} (Wang et al. 2016; Zhao et al. 2013). Furthermore, a sharp and dense peak at 808 cm^{-1} corresponds to the breathing mode of the graphitic layers constituted by conjugated triazine (or tri-s-triazine) units, which were the characteristic band of g-C_3N_4 (Xu et al. 2014). It is considered that a small amount of the amino groups remains in the composite samples synthesized.

XPS analysis for g-C_3N_4 and as-prepared composite samples are performed in Fig. 5. As described in Fig. 5a, the spectrum of g-C_3N_4 showed carbon, nitrogen and oxygen elemental signal detected at binding energies of 285, 398.4 and 533 eV. For HMCM-22, there are two peaks with binding energies of ca. 74.6, 103.2 and 533 eV, corresponding to aluminum, silicon and oxygen elements, respectively. Among them, the emergence of O species was possibly originated from the water molecules adsorbed by the material. Moreover, Si, Al, C and N elements were found in G1H1 and

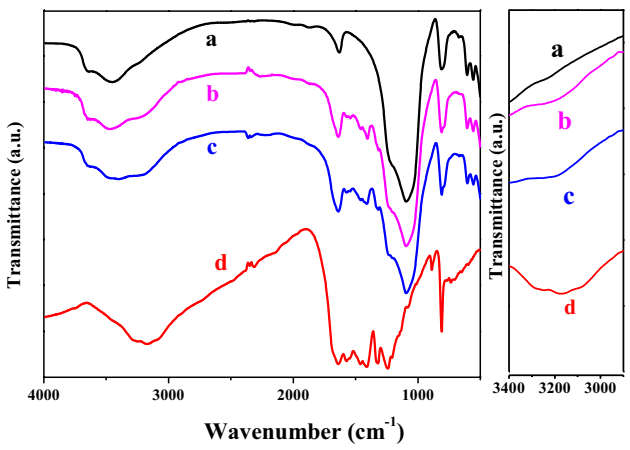

Fig. 4 FTIR spectra of g-C_3N_4, HMCM-22 and as-prepared composite samples. **a** HMCM-22, **b** G1H1, **c** G3H1, **d** g-C_3N_4

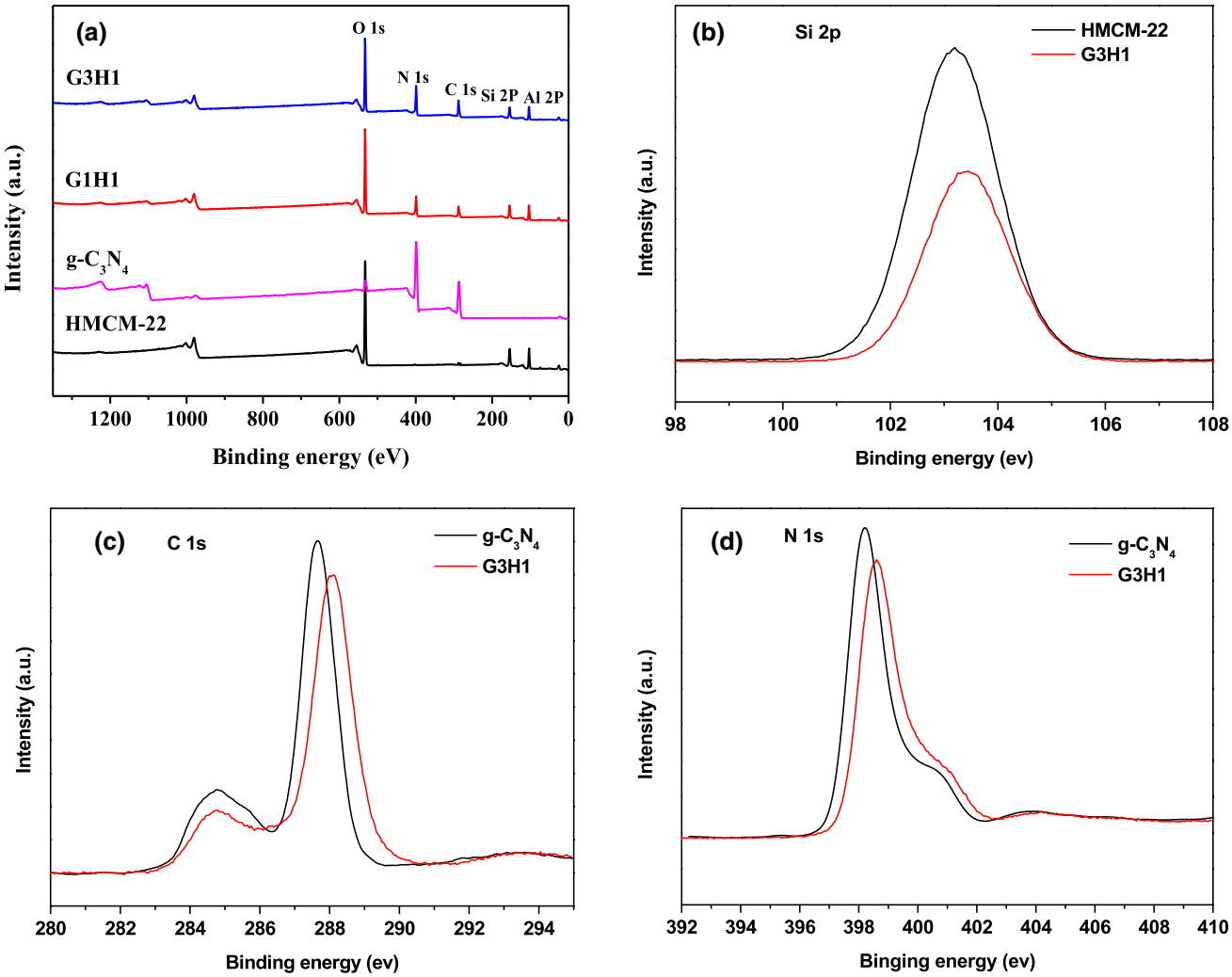

Fig. 5 Full-range XPS spectra (**a**) and Si 2P (**b**), C 1s (**c**), N 1s (**d**) spectra of g-C_3N_4, HMCM-22 and as-prepared composite samples

G3H1 catalyst, which indicated that the HMCM-22 zeolite was incorporated into the g-C_3N_4 matrix. This result was consistent with the FTIR spectra results. In order to elucidate the bonding states of g-C_3N_4 and HMCM-22, the high-resolution XPS spectra for Si 2p, C 1s and N 1s elements were also investigated and the results are shown in Fig. 5b-d. It is clearly shown that the peaks of these three elements (Si 2p, C 1s and N 1s) shift significantly. The change of binding energy indicates that the g-C_3N_4 incorporated into the lattice structure of HMCM-22, which also agrees well with the XRD results.

In order to obtain the structure and morphology of the as-prepared catalysts, SEM characterizations including the parent HMCM-22 and g-C_3N_4-HMCM-22 composite samples were performed; the images are presented in Fig. 6. It was found that the parent HMCM-22 has a flower-like and stratified structure. After introducing a small amount of g-C_3N_4 (G1H9), a small number of clumps appear on the surface of the catalyst, further increasing the amount of g-C_3N_4, and the clumps become larger. Particularly, it is difficult to see the stratified structure on G3H1 catalyst due to the large clumps covered on the surface of catalyst. EDS analysis by selecting two points from the G3H1 sample showed that there are five elements of C, O, N, Si and Al in the catalysts. However, the atomic percentage of the elements at those two points is different, which demonstrates the inhomogeneous distribution of g-C_3N_4 on HMCM-22 catalyst.

Py-FTIR was used to investigate acidity properties of the as-synthesized zeolites, which can qualitatively as well as quantitatively describe the Brönsted and Lewis acid sites. The Py-FTIR spectra after adsorbed pyridine of HMCM-22 and as-prepared composite samples are shown in Fig. 7. Py can be physisorbed or H-bonded (HPy) and can be coordinated to Lewis acid sites (LPy) or protonated on Brönsted acid sites (BPy). Parent HMCM-22 and as-prepared composite samples possess one type of

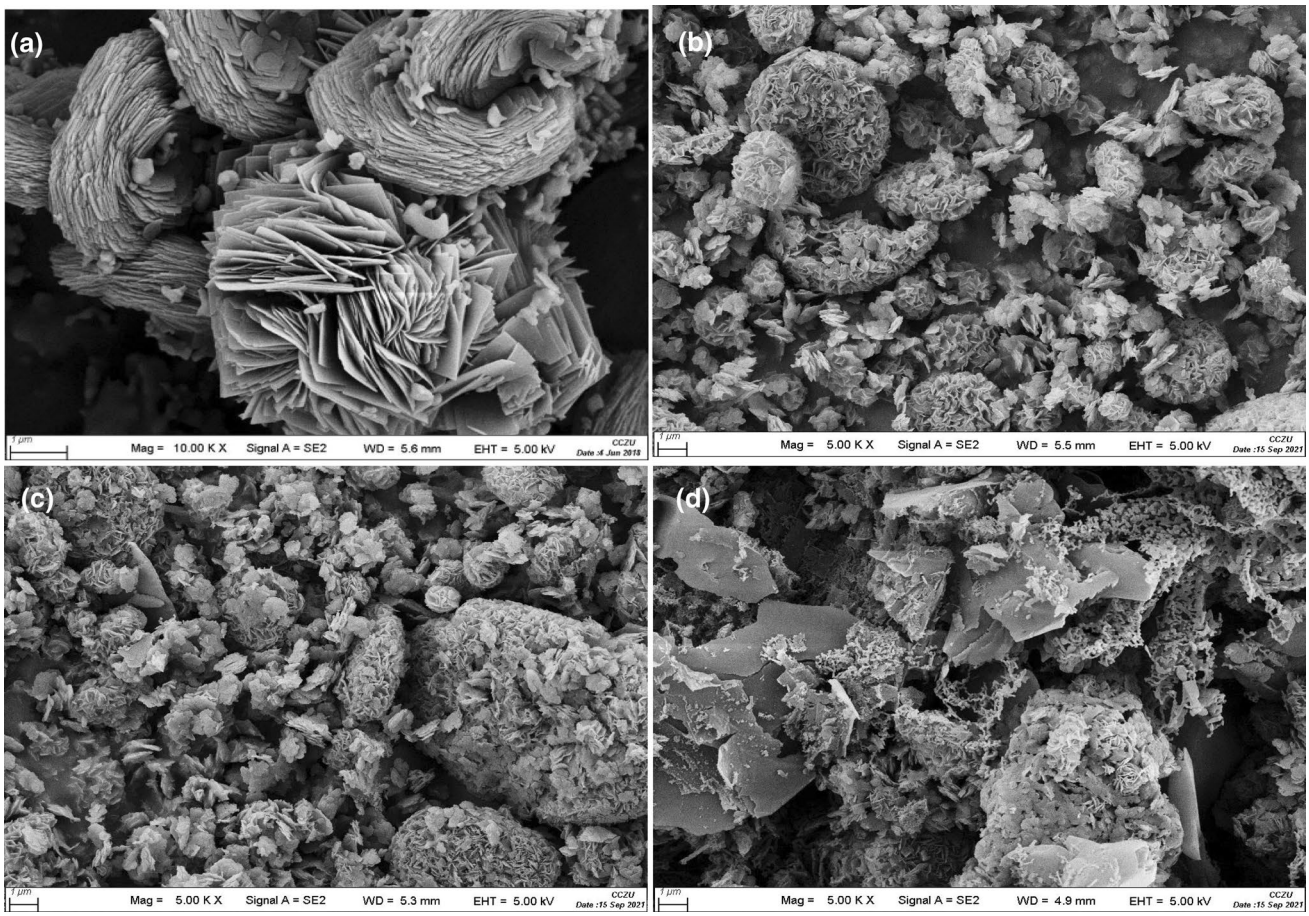

Fig. 6 SEM image of HMCM-22 (**a**), G1H9 (**b**), G1H1 (**c**), G1H3 (**d**)

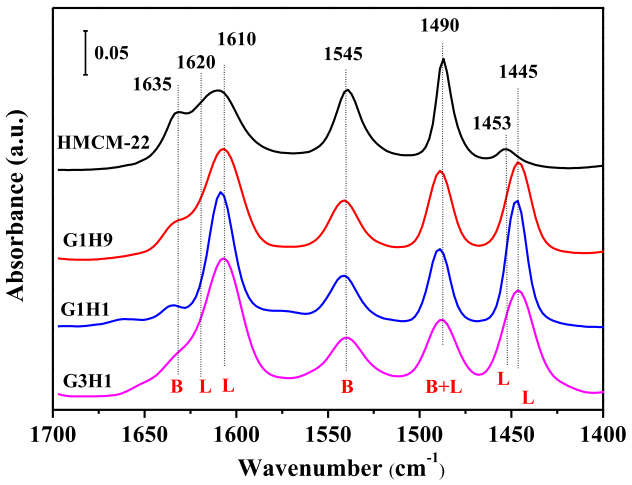

Fig. 7 Py-IR spectra after adsorbed pyridine of HMCM-22 and as-prepared composite samples

Brönsted acid site (1545 and 1635 cm^{-1}) and two types of Lewis acid sites (1453 and 1620, and 1445 and 1610 cm^{-1}) (Yaripour et al. 2015). The number of Brönsted acid sites on parent HMCM-22 was much greater than the number of Lewis acid sites. The acidity characteristics of HMCM-22 clearly changed after g-C_3N_4 introduction: the number of Lewis acid sites was larger than the number of Brönsted acid sites and the bands at 1455 cm^{-1}, corresponding to the Lewis acid sites, disappear completely in all of the as-prepared composite samples. A new strong band appears at 1445 cm^{-1}, which can be ascribed to new Lewis acid sites formed after g-C_3N_4 incorporation with HMCM-22. We found that amount of Lewis acid sites over G1H9 and G1H1 samples obviously increased with increasing g-C_3N_4 content of the composite samples from 25 to 50 wt%. Further increase in g-C_3N_4 content of the composite samples the amount of the new Lewis acid sites decreased over G3H1 sample, which can be ascribed to the partial blockage of the pore system of HMCM-22 by high g-C_3N_4 content (Xue et al. 2009). The bands at 1545 and 1635 cm^{-1} corresponding to Brönsted acid sites substantially decrease after introduction of g-C_3N_4. These results indicated that the introduction of g-C_3N_4 to HMCM-22 could effectively modify the amount of acid sites.

The isomerization reaction of MX

The catalytic results of MX isomerization over parent HMCM-22 and as-prepared composite samples are shown in Fig. 8. As for the parent HMCM-22 catalyst, the conversion of MX was 40.3%, and the ratio of *p*-xylene/*o*-xylene (PX/OX) was only 1.59. However, after introduction of g-C_3N_4, G1H9 catalysts gave lower MX conversion (32.5%) and higher PX/OX (1.91) than parent HMCM-22 catalysts. With increase in g-C_3N_4 contents from 25 to 50%, there was a downward trend in MX conversion and PX/OX increased drastically. According to N_2 adsorption and Py-FTIR results, after introducing g-C_3N_4, strength and amount of Lewis acid sites on the pore mouths and external surface of modified HMCM-22 catalysts decreased simultaneously, which resulted in the decrease in catalytic activity. However, when content of g-C_3N_4 continued to increase to 75%, the conversion of MX hardly decreased and the change of PX/OX ratio was not found. This is because the strength and amount of Lewis acid sites and external surface changed very less compared to G1H1 catalyst. Overall, G1H1 catalyst showed the highest PX selectivity than other as-prepared composite samples. Therefore, the improved PX selectivity of as-prepared composite samples was attributed to increased amounts of Lewis acid sites and effective suppression of external Brönsted acid sites. In addition, the catalytic performance of this catalyst was much higher than that of the most catalysts published in the studies, as listed in Table 2. For example, very recently, Liu et al. synthesized the Chain-like ZSM-5 zeolite and used it for the MX isomerization. The chain-like ZSM-5 zeolite exhibits relatively higher MX conversion (55%) and PX selectivity (62%) compared with the conventional ZSM-5 zeolite (Liu et al. 2021). Glotov et al. prepared Pt/Al–MCM-41/HNT(90:10)/Al_2O_3, giving a MX conversion of 23% and 69% selectivity for PX at 360 °C (Glotov et al. 2019). Mesoporous-zeolite materials were synthesized using Beta zeolite nanoparticles as precursors and applied for the MX isomerization. The author found that the MX conversion and isomerization/disproportionation ratio were related to the crystallization time, mesopores creation and the method used to produce the extra mesoporosity. The highest selectivity of PX (54%) was obtained over H-βNPs(24 h)-DHM catalyst (Chaida-Chenni et al. 2018). However, the other zeolite catalyst such as HMCM-68-MW and H-EU-1 gave a relatively low PX selectivity (< 40%) (Hao et al. 2017, Rahbari et al. 2017).

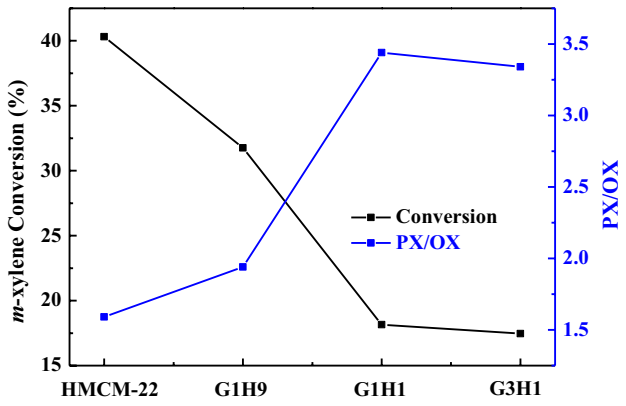

Fig. 8 Catalytic performance of parent HMCM-22 and as-prepared composite samples in MX isomerization. (Reaction condition: temperature, 673 K, WHSV=1 h^{-1}, P=0.1 MPa, $W_{catal.}$ = 1.0 g)

We also investigated the effect of weight hourly space velocity (WHSV) on MX conversion and the ratio of PX/OX over G1H1 catalyst. The MX conversion and PX/OX ratio at different WHSV (0.5-2 h^{-1}) are shown in Figure 9. When the WHSV increased from 0.5 h^{-1} to 2.0 h^{-1}, the MX conversion decreased from 23.63 to 16.57%. Shortening the exposure time will result in insufficient isomerization of MX. However, when the WHSV increased from 0.5 to 1.0 h^{-1}, the PX/OX ratio obviously increased from 2.72 to 3.44. Further increasing WHSV, the PX/OX ratio had hardly changed.

The effect of particle size of catalysts on MX isomerization reaction was also studied over the G1H1 catalyst. As shown in Figure 10, it can be found that with the particle size of catalyst increasing from 20 to 60 mesh, MX conversion (approximately 16~17%) and the PX/OX ratio (3–4) had hardly changed. Those results indicated the particle size of catalyst had no significant effect on the conversion of MX and the ratio of PX/OX in the MX isomerization reaction.

HZSM-5 with different Si/Al ratios was used instead of MCM-22 in the MX isomerization; the results are shown in Table 3. The MX conversion of HZSM-5 catalyst

Table 2 Comparison of the catalytic performance of C_3N_4-HMCM-22 and various other catalysts for the m-xylene isomerization reaction

Catalyst	Temp. (°C)	WHSV (h^{-1})	Time (h)	MX Conv. (%)	PX Selec. (%)	Reference
Chain-like ZSM-5	350	10	6	55	62	Liu et al. 2021
Pt/Al-MCM-41/HNT(90:10)/Al_2O_3	360	1	1	23	69	Glotov et al. 2019
H-βNPs(24 h)-DHM	350	1	1	23	54	Chaida-Chenni et al. 2019
HMCM-68-MW	300	10	5	46	31	Hao et al. 2017
H-EU-1	380	6	3	16	38	Rahbari et al. 2017
50%g-C_3N_4-HMCM-22	400	1	5	18	77	This work

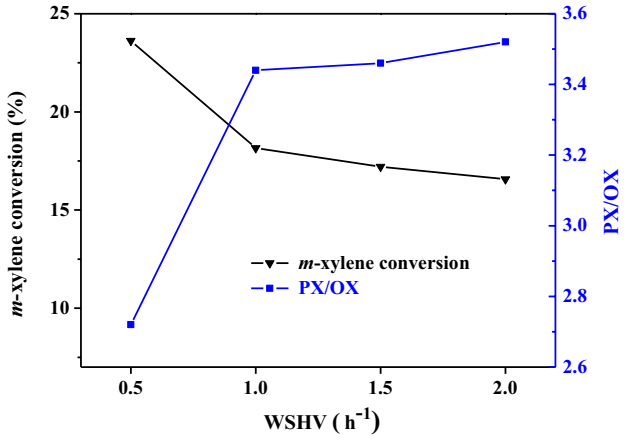

Fig. 9 Effect of WHSV on isomerization of MX over G1H1 sample. (Reaction conditions: temperature= 673 K; substrate: MX, P=0.1 MPa, $W_{catal.}$ = 1.0 g)

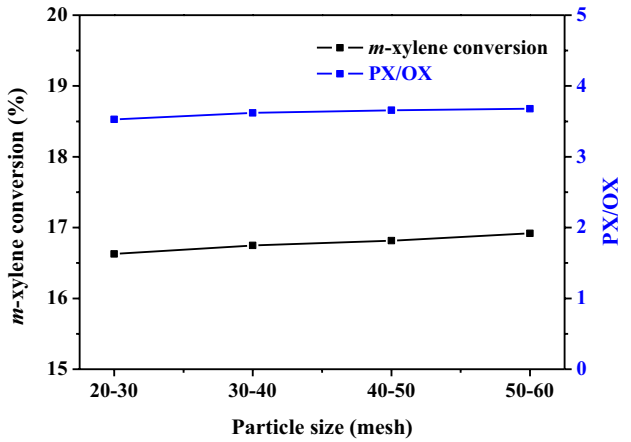

Fig. 10 Effect of catalyst size on isomerization of MX over G1H1 sample. (Reaction conditions: temperature=673 K; substrate: MX, P=0.1 MPa, $W_{catal.}$ = 1.0 g)

(47-48%) was slightly higher than that of HMCM-22 (40%), while the PX/OX ratio was much lower than that of HZSM-5 catalyst. When 50 wt% g-C_3N_4 was introduced to HZSM-5, the PX/OX ratio was slightly increased from 1.0 to 1.2 (or 1.3). For HMCM-22 catalyst, the PX/OX ratio was significantly increased from 1.6 to 3.4 when 50 wt% g-C_3N_4 was introduced. N_2 adsorption showed that the specific surface area of both HMCM-22 and HZSM-5 decreased significantly after modification with g-C_3N_4, and the total pore volume (0.25 cm^3 g^{-1}) and pore size (0.15 cm^3 g^{-1}) of g-C_3N_4/ZSM-5 catalyst were larger than that of g-C3N4-HMCM-22 catalyst. The g-C_3N_4/ZSM-5 catalyst gives much lower PX/OX ratio maybe because the kinetic diameters of aromatic molecules do not match the effective pore sizes of HZSM-5 zeolite.

Table 3 Effect of zeolite type on isomerization of MX

Catalysts	MX conversion (%)	PX/OX ratio (%)
HMCM-22	40.3	1.6
50%g-C3N4-HMCM-22	18.2	3.4
HZSM-5_50	47.3	1.0
50%g-C_3N_4/HZSM-5_50	41.3	1.3
HZSM-5_25	48.0	1.0
50%g-C_3N_4/HZSM-5_25	39.8	1.2

Reaction conditions: temperature = 673 K; WHSV=1 h^{-1}, P = 0.1 MPa, $W_{catal.}$ = 1.0 g

Conclusions

In summary, MCM-22 was proven to be an efficient and sustainable catalyst for the isomerization of MX. A series of novel graphitic carbon nitride g-C_3N_4-HMCM-22 composite catalysts were successfully prepared and characterized by XRD, N_2 physical adsorption, FTIR and XPS. Compared with parent HMCM-22 catalyst, with increasing g-C_3N_4 content, selectivity of PX increased gradually. G1H1 catalyst showed the highest PX selectivity than the catalysts with other composite catalysts, which indicated that the introduction of g-C_3N_4 to HMCM-22 could efficiently change the product distribution during MX isomerization reaction. The g-C_3N_4 can effectively suppress Brönsted acid strength at the pore mouths and external surface and increase Lewis acid sites, which resulted in the improved PX selectivity of G1H1 catalyst.

Funding This work was supported by National Natural Science Foundation of China (21878027), Advanced Catalysis and Green Manufacturing Collaborative Innovation Center (ACGM2020-08), Natural Science Foundation of the Jiangsu Higher Education Institutions (18KJA150001 and 19KJA430003), and Foundation of State Key Laboratory of High-efficiency Utilization of Coal and Green Chemical Engineering (2017-K28).

Declarations

Conflict of interest There are no conflicts to declare.

References

Amin R, Chang XQ, Liu BS (2017) Synergistic effect of CeO_2 in CH_4/CO_2 dry reforming reaction over stable xCeO_2yNi/MCM-22 catalysts. Ind Eng Chem Res 56:7445–7453. https://doi.org/10.1021/acs.iecr.7b01375

Araujo AS, Domingos TB, Souza MJB, Silva AOS (2001) m-xylene isomerization in SAPO-11/HZSM-5 mixed catalyst. React Kinet Catal Lett 73:283–290. https://doi.org/10.1023/A:1014155106147

Ayrault P, Datka J, Laforge S, Martin D, Guisnet M (2004) Characterization of the internal and external acidity of HMCM-22 zeolites. J Phys Chem B 108:13755–13763. https://doi.org/10.1021/jp048242z

Bailleul S, Yarulina I, Hoffman AEJ, Dokania A, Abou-Hamad E, Chowdhury AD, Pieters G, Hajek J, Wispelaere KD, Waroquier M, Gascon J, Speybroeck VV (2019) A supramolecular view on the cooperative role of Brönsted and Lewis acid sites in zeolites for methanol conversion. J Am Chem Soc 141:14823–14842. https://doi.org/10.1021/jacs.9b07484

Chaida-Chenni FZ, Belhadj F, Casas MSG, Márquez-Álvarez C, Hamacha R, Bengueddach A, Pérez-Pariente J (2018) Synthesis of mesoporous-zeolite materials using Beta zeolite nanoparticles as precursors and their catalytic performance in m-xylene isomerization and disproportionation. Appl Catal A-Gen 568:148–156. https://doi.org/10.1016/j.apcata.2018.10.005

Chu NB, Wang JQ, Zhang Y, Yang JH, Lu JM, Yin DH (2010) Nestlike hollow hierarchical MCM-22 microspheres: synthesis and exceptional catalytic properties. Chem Mater 22:2757–2763. https://doi.org/10.1021/cm903645p

Dusselier M, Davis ME (2018) Small-pore zeolites: synthesis and catalysis. Chem Rev 118:5265–5329. https://doi.org/10.1021/acs.chemrev.7b00738

Ghasemian N, Falamaki C, Kalbasi M (2014) Clinoptilolite zeolite as a potential catalyst for propane-SCR-NOx: performance investigation and kinetic analysis. Chem Eng J 236:464–470. https://doi.org/10.1016/j.cej.2013.10.061

Glotov AP, Artemova MI, Demikhova NR, Smirnova EM, Ivanov EV, Gushchin PA, Egazar'yants SV, Vinokurov VA (2019) A study of platinum catalysts based on ordered Al–MCM-41 aluminosilicate and natural halloysite nanotubes in xylene isomerization. Petrol Chem 59, 1226-1234 https://doi.org/10.1134/S0965544119110033

Groenewolt M, Antonietti M (2005) Synthesis of g-C_3N_4 Nanoparticles in Mesoporous Silica Host Matrices. Adv Mater 17:1789–1792. https://doi.org/10.1002/adma.200401756

Hao H, Chang Y, Yu W, Lou LL, Liu S (2017) Hierarchical porous MCM-68 zeolites: Synthesis, characterization and catalytic performance in m-xylene isomerization. Micropor Mesopor Mat 263:135–141. https://doi.org/10.1016/j.micromeso.2017.12.009

He P, Li Y, Cai K, Xiong X, Lv J, Wang Y, Huang SY, Ma XB (2020) Nano-assembled mordenite zeolite with tunable morphology for carbonylation of dimethyl Ether. ACS Appl Nano Mater 3:6460–6468. https://doi.org/10.1021/acsanm.0c00929

Jeong H, Kim Y, Lee Y, Kang M (2009) Control of acidity on the external surface of zeolite Y for m-xylene isomerization using a mechanochemical neutralization method. Korean J Chem Eng 26:371–376. https://doi.org/10.1007/s11814-009-0062-5

Leonowicz ME, Lawton JA, Lawton SL, Rubin MK (1994) A molecular-sieve with two independent multidimensional channel systems. Science 264:1910–1913. https://doi.org/10.1126/science.264.5167.1910

Li Y, Yu JH (2014) New stories of zeolite structures: their descriptions, determinations, predictions, and evaluations. Chem Rev 114:7268–7316. https://doi.org/10.1021/cr500010r

Liu S, Yang S, He J, Miao D, Yin C (2021) Efficient synthesis of chain-like ZSM-5 zeolite for the m-xylene isomerization reaction. Inorg Chem Commun 128:108564–108567. https://doi.org/10.1016/j.inoche.2021.108564

Ma XT, Zhou D, Chu X, Li D, Wang J, Song WC, Xia QH (2017) Highly selective isomerization of biomass β-pinene over hierarchically acidic MCM-22 catalyst. Micropor Mesopor Mat 237:180–188. https://doi.org/10.1016/j.micromeso.2016.09.040

Miao DY, Ding Y, Yu T, Li J, Pan XL, Bao XH (2020) Selective synthesis of benzene, toluene, and xylenes from syngas. ACS Catal 10:7389–7397. https://doi.org/10.1021/acscatal.9b05200

Min HK, Cha SH, Hong SB (2012) Mechanistic insights into the zeolite-catalyzed isomerization and disproportionation of m-xylene. ACS Catal 2:971–981. https://doi.org/10.1021/cs300127w

Qi L, Zhang YF, Conrad MA, Russell CK, Miller J, Bell AT (2020) Ethanol conversion to butadiene over isolated zinc and yttrium sites grafted onto dealuminated Beta Zeolite. J Am Chem Soc 142:14674–14687. https://doi.org/10.1021/jacs.0c06906

Rahbari ZV, Khosravan M, Kharat AN (2017) Effect of synthesis parameters on the crystallinity of EU-1 zeolite for the m-xylene isomerization reaction. Russ J Appl Chem 90:818–825. https://doi.org/10.1134/S107042721705024X

Shamzhy M, Opanasenko M, Concepción P, Martínez A (2019) New trends in tailoring active sites in zeolite-based catalysts. Chem Soc Rev 48:1095–1149. https://doi.org/10.1039/c8cs00887f

Shang YC, Yang PP, Jia MJ, Zhang WX, Wu TH (2008) Modification of MCM-22 zeolites with silylation agents: Acid properties and catalytic performance for the skeletal isomerization of n-butene. Catal Commun 9:907–912. https://doi.org/10.1016/j.catcom.2007.09.028

Shi Q, Goncalves JC, Ferreira AFP, Plaza MG, Rodrigues AE (2018) Xylene isomerization over beta zeolites in liquid phase. Ind Eng Chem Res 57:5568–5579. https://doi.org/10.1021/acs.iecr.8b00585

Talapaneni SN, Anandan S, Mane GP, Anand C, Dhawale DS, Varghese S, Mano A, Moricd T, Vinu A (2012) Facile synthesis and basic catalytic application of 3D mesoporous carbon nitride with a controllable bimodal distribution. J Mater Chem 22:9831–9840. https://doi.org/10.1039/c2jm30229b

Tsai TC, Wang I, Huang CK, Liu SD (2007) Study on the ethylbenzene and xylene conversion over modified ZSM-5. Appl Catal A 321:125–134. https://doi.org/10.1016/j.apcata.2007.01.041

Wang X, Dai WL, Wu GJ, Li LD, Guan NJ, Hunger M (2012) Phosphorus modified HMCM-22: characterization and catalytic application in methanol-to-hydrocarbons conversion. Micropor Mesopor Mat 151:99–106. https://doi.org/10.1016/j.micromeso.2011.11.008

Wang S, Wei ZH, Chen YY, Qin ZF, Ma H, Dong M, Fan WB, Wang JG (2015) Methanol to olefins over HMCM-22 zeolite: theoretical study on the catalytic roles of various pores. ACS Catal 5:1131–1144. https://doi.org/10.1021/cs501232r

Wang Y, Yokoi T, Namba S, Kondo JN, Tatsumi T (2015) Catalytic cracking of n-hexane for producing propylene on MCM-22 zeolites. Appl Catal A 504:192–202. https://doi.org/10.1016/j.apcata.2014.12.018

Wang HF, Fang LP, Yang YF, Zhang L, Wang YJ (2016) $H_5PMo_{10}V_2O_{40}$ immobilized on functionalized chloromethylated polystyrene by electrostatic interactions: A highly efficient and recyclable heterogeneous catalyst for hydroxylation of benzene. Catal Sci Technol 6:8005–8015. https://doi.org/10.1039/C6CY01270A

Wang YN, Gao Y, Xie SJ, Liu SL, Chen FC, Xin WJ, Zhu XX, Li XJ, Jiang N, Xu LY (2018) Adjustment of the Al siting in MCM-22 zeolite and its effect on alkylation performance of ethylene with benzene. Catal Today 316:71–77. https://doi.org/10.1016/j.cattod.2018.02.040

Weston SC, Peterson BK, Gatt JE, Lonergan WW, Vroman HB, Afeworki M, Kennedy GJ, Dorset DL, Shannon MD, Strohmaier KG (2019) KMM-17, a new three-dimensional zeolite with unique 11-ring channels and superior catalytic isomerization performance. J Am Chem Soc 141:15910–15920. https://doi.org/10.1021/jacs.9b07102

Wu P, Komatsu T, Yashima T (1998) Selective formation of p-xylene with disproportionation of toluene over MCM-22 catalysts. Micropor Mesopor Mat 22:343–356. https://doi.org/10.1016/S1387-1811(98)00114-0

Wu YJ, Ren XQ, Lu YD, Wang J (2008) Crystallization and morphology of zeolite MCM-22 influenced by various conditions in the static hydrothermal synthesis. Micropor Mesopor Mat 112:138–146. https://doi.org/10.1016/j.micromeso.2007.09.022

Wu X, Hu C, Zhao GQ, Yuan Y, Zhu ZR (2016) Catalytic performance of modified HMCM-22 catalysts in xylene isomerization. Chin J Chem 34:1291–1296. https://doi.org/10.1002/cjoc.201600416

Xu H, Yan J, She XJ, Xu L, Xia JX, Xu YG, Song YH, Huang LY, Li HM (2014) Graphene-analogue carbon nitride: novel exfoliation synthesis and its application in photocatalysis and photoelectrochemical selective detection of trace amount of Cu^{2+}. Nanoscale 6:1406–1415. https://doi.org/10.1039/c3nr04759h

Xu YG, Xie M, Huang SQ, Xu H, Ji HY, Xia JX, Li YP, Li HM (2015) High yield synthesis of nano-size g-C_3N_4 derivatives by a dissolve-regrowth method with enhanced photocatalytic ability. RSC Adv 5:26281–26290. https://doi.org/10.1039/c5ra01206f

Xue B, Li YX, Deng LJ (2009) Selective synthesis of p-xylene by alkylation of toluene with dimethyl carbonate over MgO-modified MCM-22. Catal Commun 10:1609–1614. https://doi.org/10.1016/j.catcom.2009.04.028

Xue B, Su J, Huang Q, Xu J, Li Y (2014) Preparation of MgO/MCM-22 catalysts by a novel two-step impregnation and their shape-selective performance in the synthesis of p-xylene. Catal Commun 45:49–53. https://doi.org/10.1016/j.catcom.2013.10.033

Yaripour F, Shariatinia Z, Sahebdelfar S, Irandoukht A (2015) Conventional hydrothermal synthesis of nanostructured H-ZSM-5 catalysts using various templates for light olefins production from methanol. J Nat Gas Sci Eng 22:260–269. https://doi.org/10.1016/j.jngse.2014.12.001

Yeong YF, Abdullah AZ, Ahmad AL, Bhatia S (2010) Synthesis, characterization and reactive separation activity of acid-functionalized silicalite-1 catalytic membrane in m-xylene isomerization. J Membr Sci 360:109–122. https://doi.org/10.1016/j.memsci.2010.05.009

Zhang WF, Liang JH, Liu YQ, SunS F, Ren XQ, Jiang M (2013) Knoevenagel condensation reaction over acid-base bifunctional MgO/HMCM-22 catalysts. Chin J Catal 34:559–566. https://doi.org/10.1016/S1872-2067(11)60493-2

Zhao P, Wang J, Chen G, Zhou Y, Huang J (2013) Phase-transfer hydroxylation of benzene with H_2O_2 catalyzed by a nitrile-functionalized pyridinium phosphovanadomolybdate. Catal Sci Technol 3:1394–1404. https://doi.org/10.1039/c3cy20796j

Zhou J, Liu Z, Li L, Wang Y, Gao H, Yang W, Xie Z, Tang Y (2013) Hierarchical mesoporous ZSM-5 zeolite with increased external surface acid sites and high catalytic performance in o-xylene isomerization. Chin J Catal 34:1429–1433. https://doi.org/10.1016/S1872-2067(12)60602-0